JOURNAL OF GEOPHYSICAL RESEARCH, VOL. 92, NO. A9, PAGES 9978–9996, SEPTEMBER 1, 1987

Z Mode Radiation in Jupiter's Magnetosphere

C. F. KENNEL, R. F. CHEN, AND S. L. MOSES

TRW Space and Technology Group, Redondo Beach, California

W. S. KURTH

Department of Physics and Astronomy, University of Iowa, Iowa City

F. V. CORONITI, F. L. SCARF, AND F. F. CHEN

TRW Space and Technology Group, Redondo Beach, California

The wideband plasma wave data acquired by Voyagers 1 and 2 in Jupiter's magnetosphere frequently contain a narrow-band emission of variable intensity whose upper frequency is below the lower-frequency cutoff of the continuum radiation. We have found examples in over 400 wideband frames taken outside the plasma sheet between 20 and 90 R_J from the planet in the dayside and nightside magnetosphere. The narrow-band emissions do not appear to be electrostatic waves. If they are electromagnetic, they can be identified by relating their frequencies to the fundamental frequencies of the ambient plasma and the solutions to the cold plasma dispersion relation. Since the electron plasma frequency was not measured at the rate and accuracy we need, we attempt to infer it by testing two hypotheses about the lower-frequency cutoff of the continuum. By analogy with terrestrial observations, we assume that the continuum cutoff is either at the plasma frequency or the right-hand cutoff frequency at which the right-hand polarized extraordinary mode cuts off. The measured electron cyclotron frequency then enables us to determine the wave mode of the narrow-band emissions. More consistent results followed from assuming the continuum cut off at the right-hand frequency. Under this assumption the narrow-band emission falls between the left-hand cutoff frequency and upper hybrid frequencies, which identifies the waves as the slow branch of the X mode, or the so called Z mode. This also implies that the continuum is comprised of R-X mode waves where the Z mode is observed as a separate band, since the L-O mode would fill the gap between the Z mode and continuum bands. As Voyager 1 approached the plasma sheet on March 8, 1979, the Z mode intensified and then disappeared on plasma sheet entry. We interpret this as evidence of local Z mode generation.

1. INTRODUCTION

Early in the analysis of data from the Voyager plasma wave instrument (PWS) obtained within Jupiter's magnetosphere, *Gurnett et al.* [1980] pointed out the existence of an intense, narrow-band emission that was lower in frequency than the Jovian continuum radiation and separated from the continuum spectrum by a distinct gap. Since in their case this emission appeared below the electron cyclotron frequency (f_c), it did not fit into the known categories of electrostatic instabilities and was therefore regarded as a mystery. Continued processing of the more than 11,000 frames of wideband plasma wave data acquired by Voyagers 1 and 2 at Jupiter has revealed over 400 examples of these emissions. In this paper we will outline their general phenomenology and present our conclusions on the nature and significance of these waves.

These intense narrow-band emissions are a common but highly variable feature of Jupiter's middle magnetosphere and have been found outside the plasma sheet between 20 and 90 R_J from the planet. Although the amplitude of the continuum radiation to which they are related changes slowly in time, the narrow-band emissions are highly variable, with their power fluxes varying by at least 4 orders of magnitude. The power densities integrated over the bandwidths of the most intense narrow-band emissions can be more than an order of magnitude larger than those of the much broader band continuum.

The fact that the frequency of the narrow-band emission does not correlate with specific multiples of f_c suggests to us that the narrow-band emissions are electromagnetic rather than electrostatic waves. Identifying the modes that propagate in this band requires fitting the observations to the solutions of the cold-plasma, electromagnetic dispersion relation. However, this necessitates a more precise and rapid determination of the plasma frequency (f_p) than can be obtained from the Voyager plasma science (PLS) instrument. To overcome this problem we apply different interpretations of the lower-frequency cutoff of the continuum band to derive f_p and look for consistencies in the resulting narrow-band emission frequencies. The best results were obtained when the continuum cutoff was set equal to the right-hand cutoff frequency (f_R). Under this assumption the narrow-band emission consistently occurs between the upper hybrid frequency (f_H) and the left-hand cutoff frequency (f_L) (these frequencies will be defined rigorously in the next section). This implies that the narrow-band emission is probably in the Z mode (the slow branch of the X mode) but also requires that L-O mode radiation be absent from the continuum when the Z mode is observed as a distinct band.

In section 2 we discuss how we selected events for further study, since the selection procedure must be taken into account in understanding our results. Two examples of wideband data containing a broadband continuum, a gap, and the narrow-band emission are introduced, and by comparing the

Paper number 7A8935.
0148-0227/87/007A-8935$05.00

spectral density of the broadband continuum previously reported by *Gurnett et al.* [1980] with that measured when the narrow-band emissions are present, we are able to demonstrate that the lower-frequency band corresponds to an entirely separate emission, while the higher-frequency radiation is the continuum radiation previously reported by *Gurnett et al.* [1980].

In section 3 we outline how we deduced the cutoff of the continuum and identified the narrow-band emission as the Z mode. By locating these waves on the Clemmow-Mullaly-Allis (CMA) diagram [*Stix*, 1962], we discuss the implications of this interpretation of the nature of electromagnetic radiation in Jupiter's magnetosphere.

In section 4 we briefly indicate where Z mode radiation was found in Jupiter's magnetosphere and also where our selection procedure would have made it difficult to find.

In section 5 we discuss our Z mode observations during the plasma sheet crossing of March 8, 1979, where we believe we have identified at least one generation region for the Z mode.

In section 6 we summarize our arguments and relate our observations to existing theories of Z mode generation in Earth's magnetosphere.

2. Selection of Events

Plate 1 shows two examples of the type of event we have selected for study in this paper. The top and bottom panels present 30 s of wideband plasma wave data from March 3, 1979 (Voyager 1), and July 6, 1979 (Voyager 2). Frequency is given on the vertical axis, and wave intensity is indicated by color (red for the most intense and blue for the least intense signals). A broadband continuum is evident at the higher-frequency portions of both panels. The continuum has a sharp lower-frequency cutoff and is separated from the lower-frequency narrow-band emission by a gap in which no waves are detected. In the top panel the weak narrow-band emission faded, disappeared, and then reintensified, while the continuum remained at a constant intensity throughout the time interval shown, implying that the broadband and narrow-band emissions behaved independently of one another. In the bottom panel the narrow-band emission intensified as time progresses. Although the broadband continuum appears to have diminished in intensity and bandwidth as the intensity of the narrow-band line increased, this was because of the automatic gain control (AGC) amplifier in the broadband data system, which normalizes each spectrum of the amplitude of the strongest signal.

It should be noted that the narrow "absorption line" in the top panel and the "emission line" in the bottom panel at 2.4 kHz are due to a spacecraft signal emanating from the power supply which was only partially filtered out. The short, intense, very low frequency bursts are also due to spacecraft interference from the low-energy charged particle (LECP) analyzer stepper motor [*Scarf et al.*, 1981]. These artifacts, which will also appear in the data presentations to come, have no scientific significance. They can, however, reduce the apparent amplitude of the continuum and other waves modes due to the AGC effect.

Figure 1 shows two examples of calibrated spectra obtained from the wideband data system and averaged over 4 s. We have superposed on the spectrum in the top panel (March 1, 1979) the dayside continuum amplitude plotted by *Gurnett et al.* [1980, Figure 4]. The spectrum in the bottom panel, which was acquired when Voyager 1 was in the nightside of Jupiter's magnetosphere, is compared with a nightside continuum spectrum [*Gurnett et al.*, 1980].

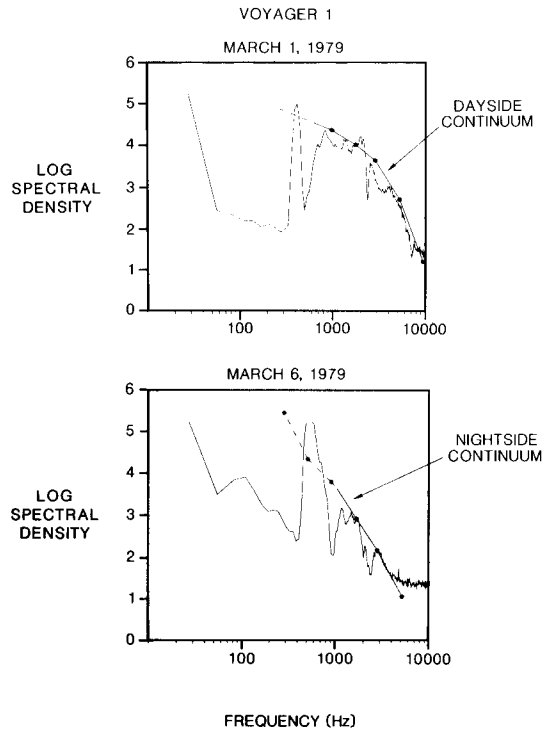

Fig. 1. Narrow-band plus continuum spectra. Two examples of spectra acquired from the wideband data system in the dayside (top panel) and nightside (bottom panel) of Jupiter's magnetosphere are shown. Superposed on the spectra are the measurements of the continuum spectrum made by *Gurnett et al.* [1980]. The dashed lines indicate the extension of the continuum spectrum to frequencies below which it was detected on March 1 and March 6, 1979.

Gurnett et al.'s [1980] continuum spectra were not taken at the same times as the individual wideband spectra shown. However, the shape of the continuum spectrum is roughly invariant, and its amplitude is gently modulated on 5- to 10-hour time scales [*Kurth et al.*, 1986]. Our primary interest here is to show that the spectral shape of the continuum at frequencies above those of the narrow-band emissions is similar to what has been found previously, whereas the narrow-band emission appears to be distinctly different.

The examples in Figure 1 suggest that the spectral density of the narrow-band emission can be comparable with that of the continuum radiation, and in the case of the nightside observation in the bottom panel, the integrated narrow-band amplitude exceeded that of the projected continuum spectrum at that frequency

The fact that the narrow-band and continuum spectral densities in these examples are comparable is partially due again to the selection process. If the narrow-band emission were significantly less intense than the continuum, it would not have been selected for study from inspection of photographically displayed wideband data such as that in Plate 1. On the other hand, if the narrow-band emission were very much more intense than the continuum, the AGC amplifier would have suppressed the continuum in the wideband frames.

In sum, we searched the wideband plasma wave data for events that display a broadband continuum with a lower-frequency border, a gap wide enough to be identified, and a

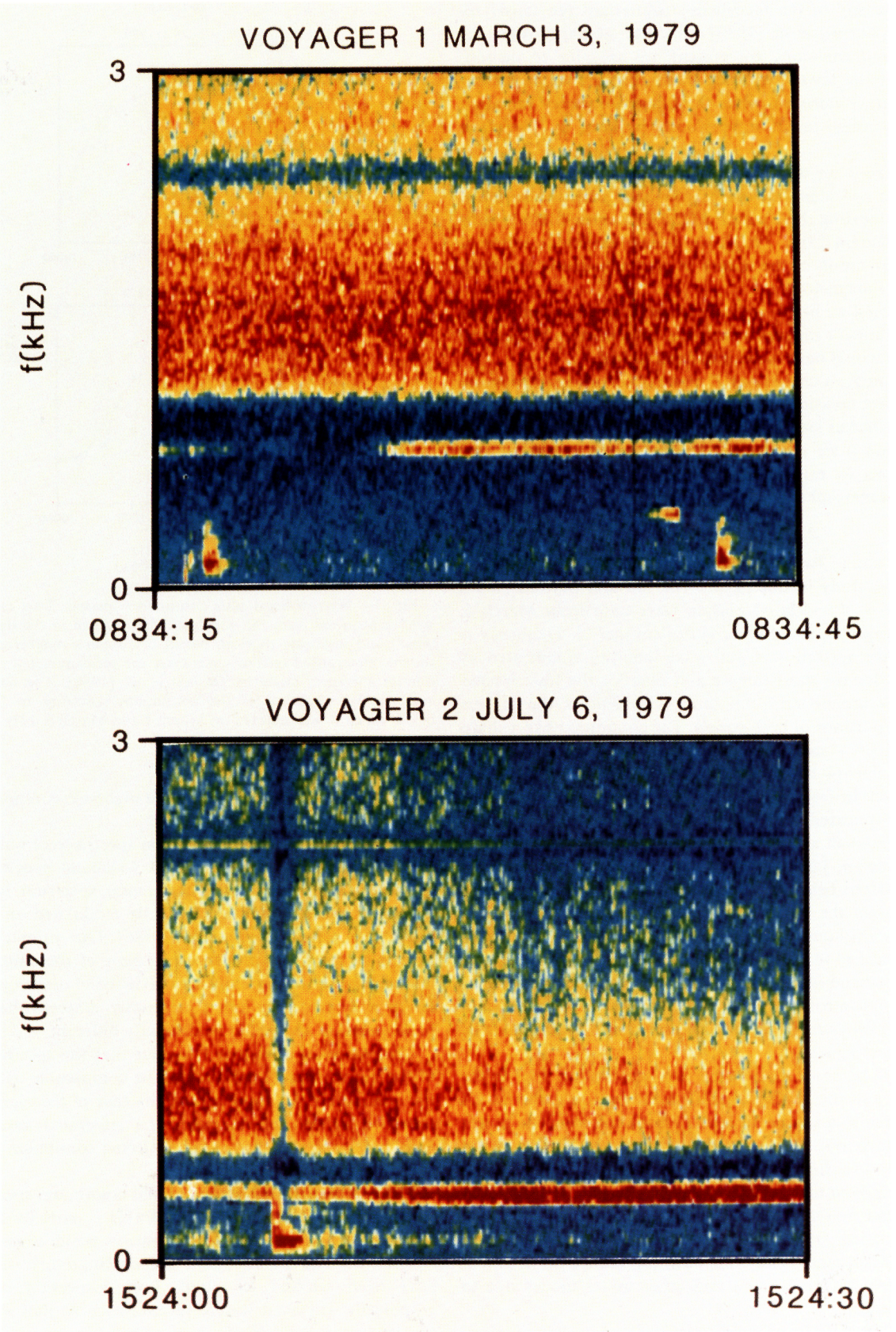

Plate 1. Examples of narrow-band emissions. This plate shows color spectrograms of two examples of the events studied in this paper. Intensity is displayed on a color scale that ranges from blue (least intense) to yellow to red (most intense). Because of the automatic gain control amplifier, the intensities are not absolute. The top panel shows a high-frequency band of continuum radiation of roughly constant intensity, with a sharp lower-frequency cutoff, a gap, and an intermittent narrow-band emission. An AGC effect is apparent near 1524:04 spacecraft event time in the lower panel, where the spacecraft interference at low frequencies was so intense that it blanked out the continuum momentarily. Moreover, as the intensity of the narrow-band emission increased, the intensity and bandwidth of the continuum appeared to decrease.

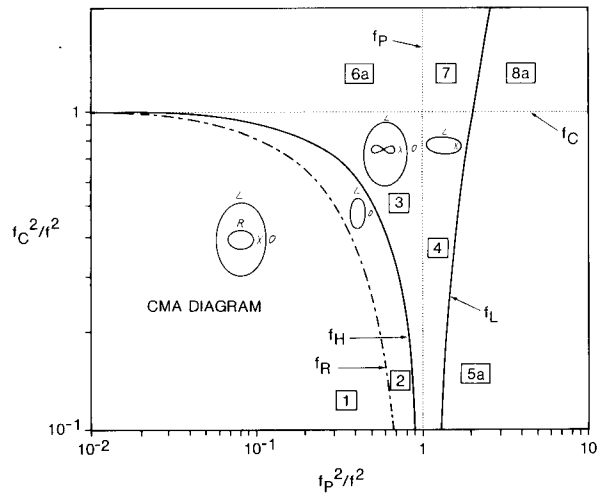

Fig. 2. CMA diagram. This figure shows the portion of the CMA diagram [*Stix*, 1962] relevant to our study. In order to locate a given wave in the CMA diagram, it is necessary to know the wave frequency f, the electron cyclotron frequency, f_c, and the electron plasma frequency, f_p. This portion of the CMA diagram is divided into eight regions, numbered according to *Stix* [1962], by the five characteristic frequencies, f_c, f_p, the upper hybrid frequency, f_H, and the right- and the left-hand cutoff frequencies, f_R and f_L. Phase velocity surfaces are sketched in each region, and the polarizations for parallel (vertical) propagation (right- to left-hand circular, R or L) and perpendicular (extraordinary or ordinary mode, X or O) propagation are indicated.

narrow-band emission whose intensity must be roughly comparable to that of the broadband continuum. The data so chosen were then subjected to further analysis. Thus we have studied a selected data set. The implications of our selection procedure will become clearer after we complete the analysis of these data in the following sections.

3. Identification of the Narrow-Band Emission Mode

Although the amplitudes of the narrow-band waves may vary and can often be more intense than the continuum, they do not exhibit the bursty character associated with locally generated and propagating electrostatic waves. Their morphological features—their lack of rapidly drifting temporal structure, their lack of harmonically related structures, and the absence of a clear association of their frequencies with the electron cyclotron frequency, its harmonics, and variations thereof—make them dissimilar to the electrostatic waves found in Earth's and Jupiter's magnetospheres. Thus we will assume the narrow-band emissions are electromagnetic and compare their frequencies with the predictions of the cold-plasma dispersion relations. Figure 2 shows the portion of the Clemmow-Mullaly-Allis diagram pertinent to our wave observations, using the solutions to the cold plasma, electromagnetic dispersion relation given by *Stix* [1962]. The CMA diagram summarizes the properties of these solutions in a $(f_c^2/f^2, f_p^2/f^2)$ parameter space, where f is the wave frequency, f_c is the local electron cyclotron frequency, and f_p is the local electron plasma frequency. (We will consider those wave frequencies for which the ions may be treated as a constant charge-neutralizing background.) As is discussed in detail by *Stix* [1962], the CMA diagram is divided into distinct regions according to where the waves propagating either parallel or perpendicular to the ambient magnetic field have either resonances ($n^2 \to \infty$) or cutoffs ($n^2 = 0$) where n is the index of refraction. A left-hand (L) and a right-hand (R) circularly polarized mode propagate parallel to the magnetic field. When ion motions may be neglected, their dispersion relations are

$$n_L^2 = L = 1 - \frac{f_p^2}{f(f+f_c)} \tag{1a}$$

$$n_R^2 = R = 1 - \frac{f_p^2}{f(f-f_c)} \tag{1b}$$

The R mode has a resonance ($n^2 \to \infty$) at $f = f_c$. The R and L modes have cutoffs ($n^2 = 0$) at the right- and left-hand cutoff frequencies,

$$f_R = \frac{f_c}{2} + \left(f_p^2 + \frac{f_c^2}{4}\right)^{1/2} \tag{1c}$$

$$f_L = -\frac{f_c}{2} + \left(\frac{f_c^2}{4} + f_p^2\right)^{1/2} \tag{1d}$$

Hereinafter, we will use the terminology right-hand and left-hand cutoff frequencies to denote the frequencies at which the right-hand and left-hand parallel propagating waves have zero index of refraction.

Two modes, termed the ordinary (O) and extraordinary (X) modes, propagate perpendicular to the magnetic field. Their dispersion relations are

$$n_O^2 = 1 - f_p^2/f^2 \tag{2a}$$

$$n_x^2 = \frac{(f^2 - f_c^2)RL}{f^2 - f_H^2} \tag{2b}$$

where R and L are defined in (1a) and (1b) and f_H is the so-called upper hybrid frequency

$$f_H^2 = f_p^2 + f_c^2 \tag{2c}$$

Note that $f_R \geq f_p \geq f_L$. The O mode cuts off at the plasma frequency ($f = f_p$), and the X mode has a resonance at the upper hybrid frequency.

The five characteristic frequencies, f_R, f_H, f_p, f_c, and f_L divide the high-frequency portion of the CMA diagram shown in Figure 2 into distinct regions. The plasma and cyclotron frequencies are the vertical and horizontal dotted lines, respectively. The upper hybrid frequency is indicated by the solid line to the left of the plasma frequency. The right-hand and left-hand cutoff frequencies are the dot-dash line to the left of the hybrid frequency and the solid line to the right of the plasma frequency, respectively. The numbers in square boxes denote the regions of the CMA diagram defined by *Stix* [1962]. The sketches inside regions 1–4 summarize the propagation properties of the wave modes predicted by the cold-plasma electromagnetic dispersion relation. The small drawings characterize the dependence of the phase velocity on the angle between the wave propagation vector and the direction of the external magnetic field, which is taken to be vertical. The small letters indicate the wave polarization, right-hand (R) or left-hand (L) circularly polarized propagating parallel to the magnetic field and ordinary (O) or extraordinary mode (X) propagating perpendicular to the magnetic field.

Free-space propagating radio waves of all polarizations can exist simultaneously in region 1 but have different low-frequency cutoffs. The continuum radiation at Earth has been

shown to be a mixture of free-space *R-X* and *L-O* mode waves [*Gurnett and Shaw*, 1973; *Shaw and Gurnett*, 1980], and polarization measurements from spinning spacecraft have identified two cutoff frequencies. As can be seen in the CMA diagram, the *R-X* mode has a cutoff at f_R, below which only the *L-O* mode can propagate. At Earth the *L-O* mode component of the continuum cuts off at f_p [*Shaw and Gurnett*, 1980], and since $f_R > f_p$, the low-frequency cutoff of the continuum is often used to determine the local plasma density.

The *Z* mode [*Lembege and Jones*, 1982] which will be of interest is the *X* mode branch which lies in regions 3 and 4 between the upper hybrid and left-hand cutoff frequencies. Note that the *Z* mode is *X* only in region 3 and *L-X* in region 4. It is *R-X* in region 6a and *L-X* in region 7.

Of the three parameters, f, f_p, and f_c, needed to locate a given wave in the CMA diagram, the plasma wave instrument measures the wave frequency, f, directly, and the electron cyclotron frequency, f_c, can be derived from the Voyager magnetometer measurements. However, the PLS does not determine the plasma frequency to the 100-Hz accuracy we will need and requires 96 s (twice the duration of a wideband frame) to complete one measurement. Thus we do not know the electron plasma frequency. In order to locate the narrow-band emission in the CMA diagram, we will test different assumptions about the cutoff frequency of the continuum to see which provides the most consistent interpretation of narrow-band emission.

The two most logical choices for the continuum cutoff are f_R and f_p. Plate 2 shows an example where we have tried both interpretations and then derived the other fundamental frequencies. The measured cyclotron frequency, which is indicated by "C," is obviously the same in both solutions. The solution set labeled by primes assumes the continuum cuts off at f_p, labeled by "P"; the other, unprimed, solution set assumes the continuum cuts off at f_R, indicated by "R." The other important quantities, f_H and f_L, are labeled by "H" and "L," respectively. As one can see, in the conventional ("primed") analysis the narrow-band emission lies above f_c and below f_L, which is a region of no propagation for electromagnetic waves. The alternate analysis puts the emission largely in the *Z* mode band between f_L and f_H. The peak in the low-frequency band occurs near our estimate of f_H, and the intensity falls very rapidly above this frequency.

Plate 3 shows another, more complex example, which we have also subjected to the above analysis. In this case the low-frequency cutoff of the continuum band increased with time, while magnetometer data shows the *B* field remained constant. The narrow-band emission was present initially, then disappeared as the continuum cutoff frequency increased, and finally reappeared as a short burst with a higher frequency. The labels R, H, etc., to the left- and right-hand sides of the wideband frame denote our solutions for the first and second narrow-band emissions, respectively, assuming the continuum cut off at f_R. The spectral density for the second narrow-band emission is displayed in the lower right panel. Both the first and second narrow-band emissions lay within the *Z* mode band, in other words, between the left-hand cutoff frequency and the upper hybrid frequency. The spectrum shown in the lower left panel corresponds to a time when no *Z* mode was present; the characteristic frequencies could not be obtained for this interval.

The magnetic field strength did not change over the time interval displayed in Plate 3, while the plasma density clearly increased. It is significant that the narrow-band emission increased in frequency. Thus the narrow-band emission was not keyed to the magnetic field, as one might expect for an odd half-harmonic electrostatic wave.

Plates 4 and 5 complete the analysis of the events in Plate 1. In Plate 4 the narrow-band emission was present throughout the 48-s data display and intensified as time progressed. The 4-s average spectrum in Plate 4 was taken at the time when the narrow-band emission was the most intense, as may be inferred from the strong AGC suppression of the continuum band between seconds 36 and 40. In this case the narrow-band emission had a peak spectral density 2 orders of magnitude larger than the peak spectral density of the continuum. Our solutions for the right-hand (R) and left-hand (L) cutoff frequencies and the upper hybrid frequency (H) are shown. Once again, the narrow-band emission filled the allowed range of frequencies for the *Z* mode. Plate 5 shows an intermittent *Z* mode emission which had a much smaller frequency bandwidth than did the cases shown earlier. Its spectral density was comparable with that of the continuum. In this case the narrow-band emission was contained within, but did not fill, the range of frequencies available to the *Z* mode.

The individual spectra presented earlier seemed to indicate that the *Z* mode amplitude tended to peak near the upper hybrid frequency, whereas the rougher frequency estimates obtained from wideband displays plotted in Figure 3 do not show this tendency. In the next section we will show spectra taken near a possible *Z* mode source which peak at the local cyclotron frequency.

Figure 3 summarizes the results of numerous analyses of wideband data such as those shown in the previous figures. In the top panel of Figure 3, we assumed that the continuum radiation cuts off at f_R and then plotted the center frequencies f of the narrow-band emissions as a function of f/f_c and f/f_p. The allowed parameter range for the *Z* mode, which is above the left-hand cutoff frequency f_L and below the upper hybrid frequency f_H, is shaded. In the middle panel of Figure 3, we plotted the same data in the same format, but now assuming that the continuum cuts off at the plasma frequency f_p.

If the continuum cuts off at f_R, then nearly all the emission frequencies lie in the *Z* mode band, and the remaining ones are sufficiently near the *Z* mode band that errors in our visual estimation of the center frequencies may account for the discrepancies. On the other hand, if the continuum cuts off at f_p, the data are grouped around the left-hand cutoff frequency, with a significant portion below f_L, where electromagnetic waves would not be expected.

We can also ask whether the bandwidth of the observed emissions, estimated visually from wideband data displays, fits within the *Z* mode band, as the individual analyses in Figure 2 and Plates 2–5 suggest. The bottom panel of Figure 3 shows a number of bandwidth estimates, taken from a randomly selected subset of our narrow-band emission events, assuming that the continuum cuts off at f_R. By and large, the observed bandwidths are in the *Z* mode band, but it is clear that the emissions do not always fill the band.

Figure 3 also reveals the range of normalized emission frequencies isolated by our selection procedure. The top panel of Figure 3 indicates that we found *Z* mode emissions in the ranges $0.8 \leq f/f_p \leq 1.8$ and $0.5 < f/f_c < 7$. The large majority of the *Z* mode emissions we found were above the electron cyclotron frequency, and our sample shows no obvious relationship to the cyclotron frequency, its harmonics, or half-

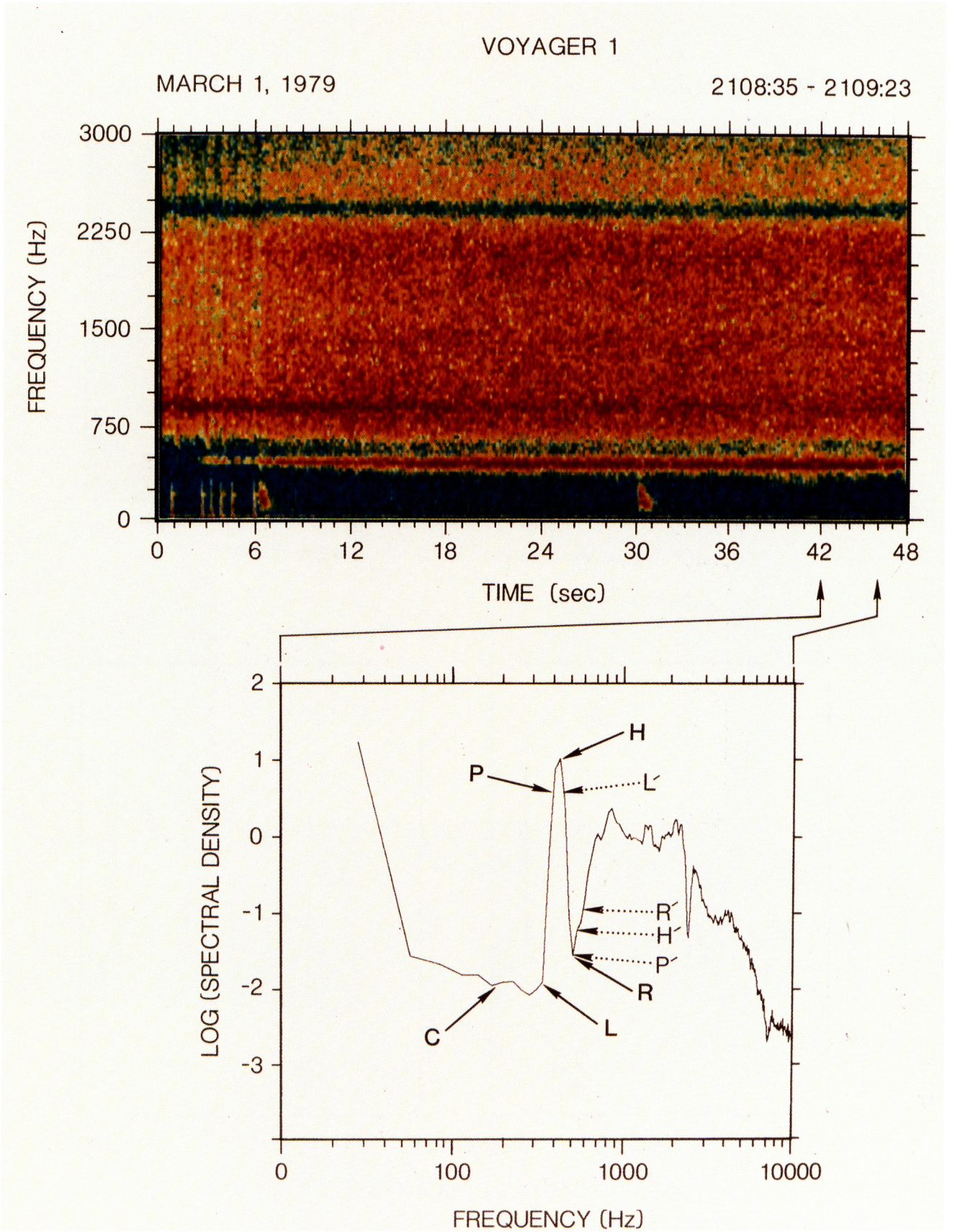

Plate 2. Two possible CMA solutions. The top panel shows a wideband frame containing continuum radiation, a gap, and a narrow-band emission of variable intensity. The bottom panel shows a 4-s average spectrum obtained between seconds 42 and 46 of the above data display. The instantaneous cyclotron frequency is labeled by C. The CMA solution labeled by primes was obtained assuming that the continuum cut off at the plasma frequency (P); the solution in bold letters assumed that the continuum cut off at the right-hand cutoff frequency (R). The left-hand cutoff and upper hybrid frequencies are denoted by L and H, respectively.

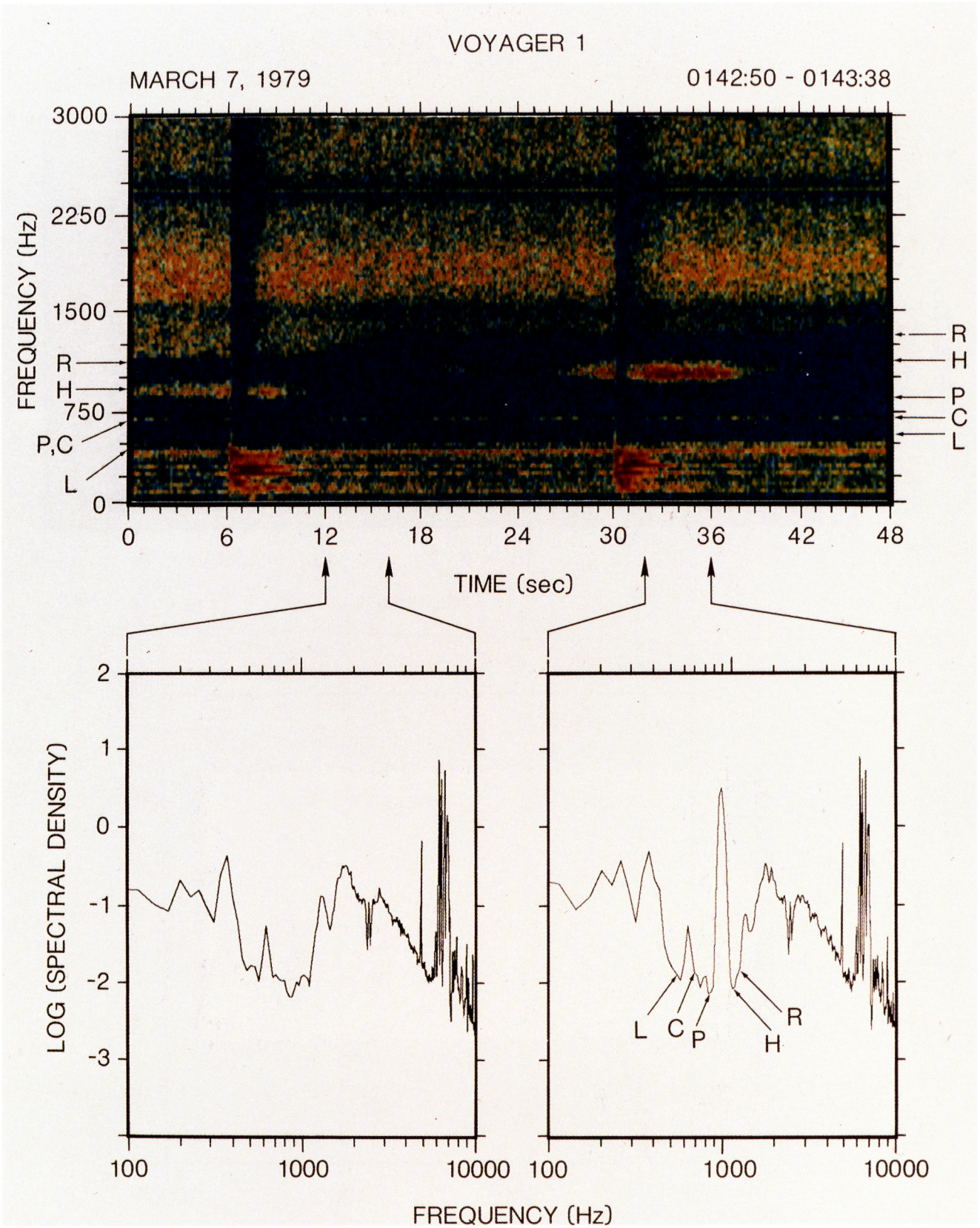

Plate 3. CMA solutions for a complex event. The format of this diagram is similar to that of Plate 2. The top panel shows an event in which the continuum cutoff frequency increased with time and the intermittent narrow-band emission frequency also increased. The labels R, H, P, C, and L denote the CMA solutions corresponding to the first (left side) and second (right side) narrow-band emissions. We assumed that the continuum cuts off at f_R. The lower left panel shows a 4-s average spectrum acquired just after the first narrow-band emission ended. The lower right panel shows the spectrum, plus the CMA solution, for the most intense portion of the second narrow-band emission.

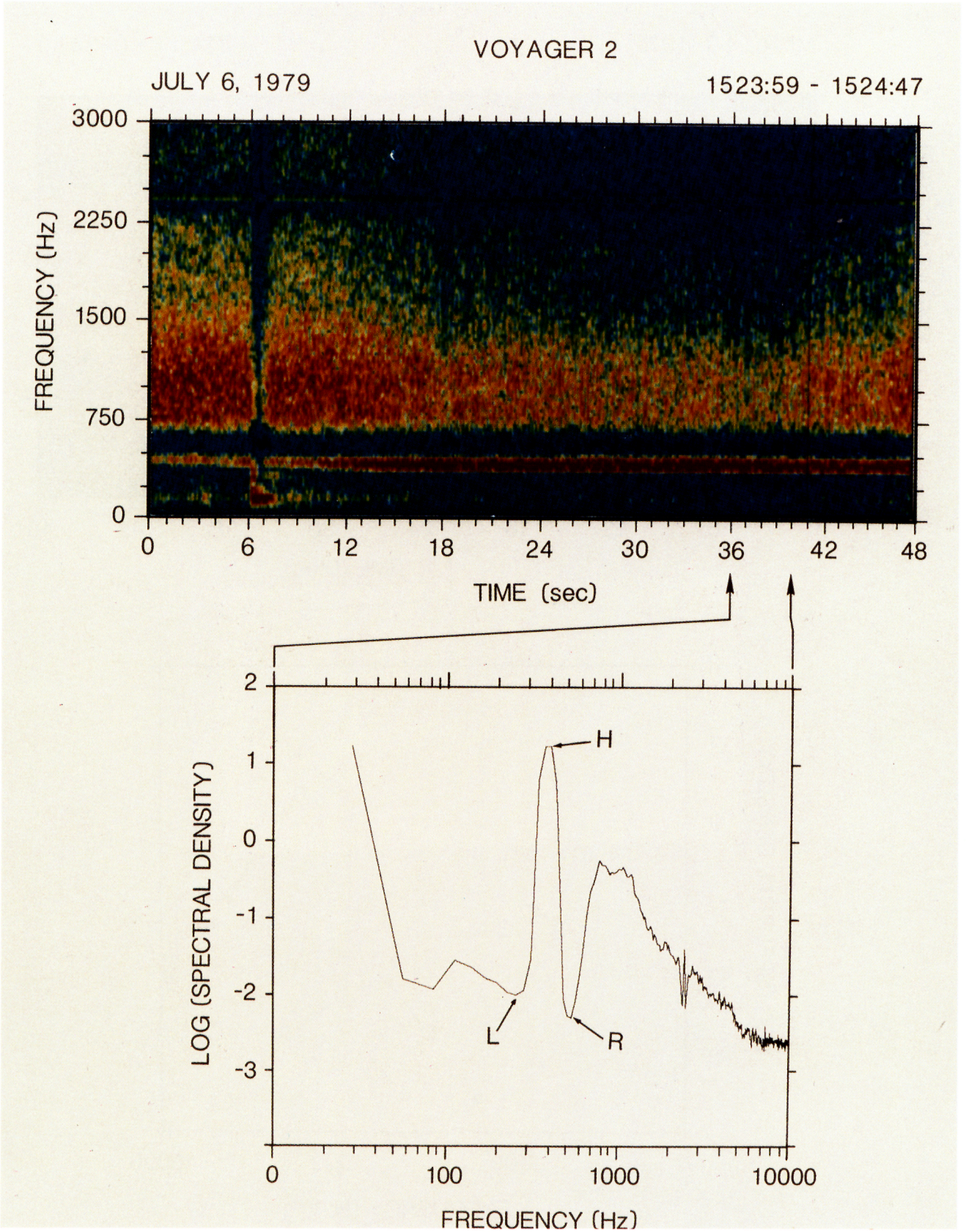

Plate 4. Intense Z mode event. This plate completes the analysis of the bottom panel of Plate 1. The 4-s spectrum at the bottom was acquired when the narrow-band emission was the most intense. Its peak spectral density was about 2 orders of magnitude larger than that of the continuum. Our CMA solution for the characteristic frequencies f_R, f_H, and f_L are also shown. The narrow-band emission filled the entire frequency range available to the Z mode.

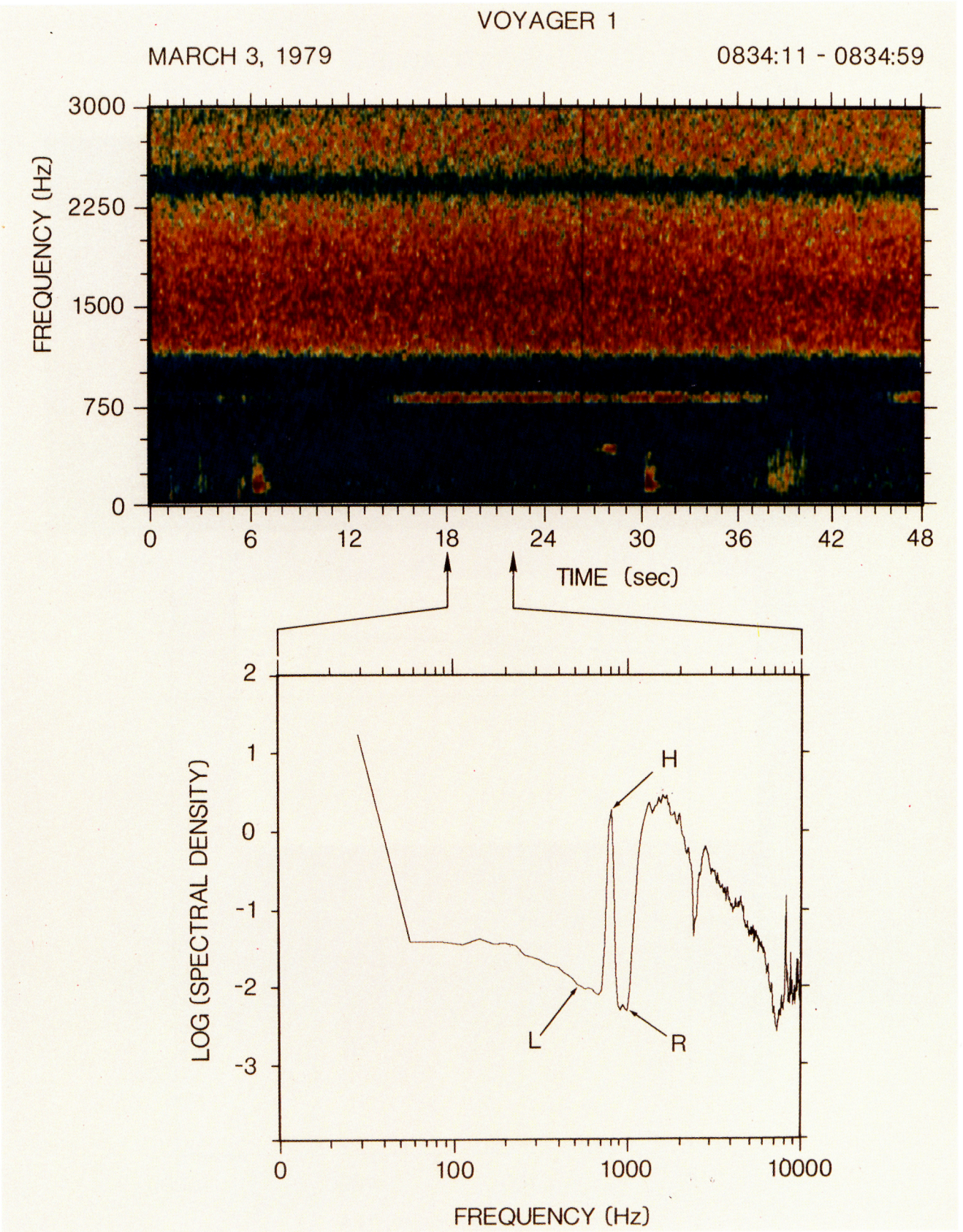

Plate 5. A narrow-band Z mode event. This plate completes the analysis of the top panel of Plate 1. In this case the Z mode emission does not fill the frequency range between f_L and f_H.

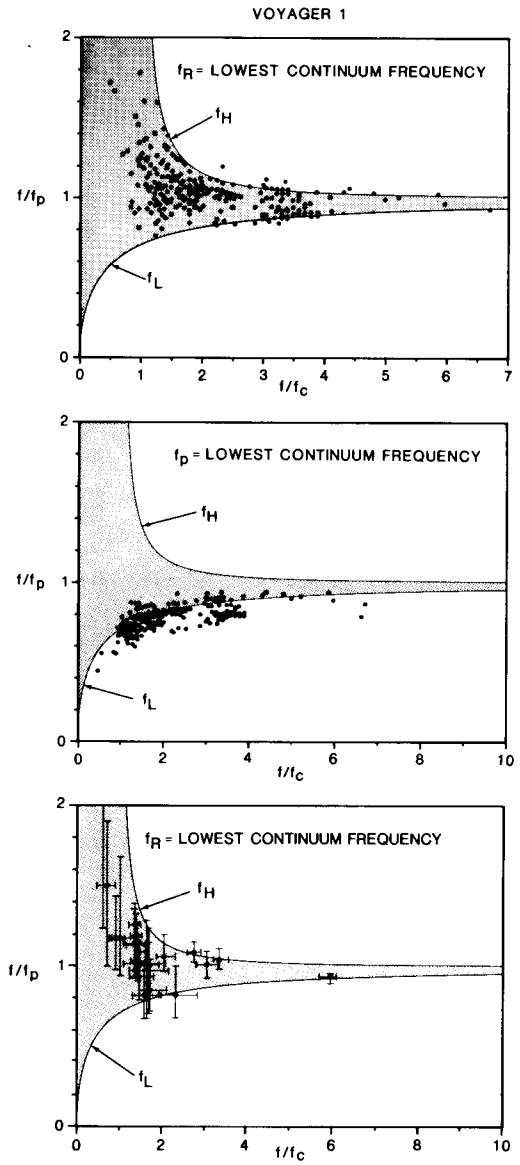

Fig. 3. Ensemble of CMA solutions for narrow-band emission center frequencies and bandwidths. The top panel shows the CMA solutions obtained assuming the continuum cuts off at f_R for center frequencies of the narrow-band emissions that were visually estimated from wideband frequency-time displays. The middle panel shows the CMA solutions obtained for the same center frequencies assuming that the continuum cuts off at f_p. The Z mode propagation band, which is bounded below by f_L and above by f_H, is shaded. The bottom panel shows visually estimated bandwidths in the same format as the top panel of Figure 3, assuming the continuum cuts off at f_R. The bandwidths fall within the Z mode propagation band, to the accuracy that we can estimate the bandwidths from frequency-time data displays.

harmonics. Furthermore, since the majority of our events had $f > f_c$, we can say that it was certainly region 2 *L-O* mode radiation that had to be absent in order for a gap to separate the lower border of the continuum from the Z mode band. About half the Z mode emissions in the top panel were above the local plasma frequency, and half were below it. Thus the Z mode emissions we found were roughly equally divided between regions 3 and 4 of the CMA diagram.

It should be emphasized that we did not analyze a properly weighted "deep" sample of data, but we simply plotted the inferred center frequencies of those events we selected to study. It would have been difficult to find events either when $f_p \gg f_c$ or when $f_c \gg f_p$, for then f_R and f_H would have been close together, and the gap between the lower-frequency cutoff of the continuum and the Z mode band would have been hard to identify. This may be seen by computing the normalized bandwidth of the gap between the continuum cutoff and the Z mode band in the limits of $f_p \gg f_c$ and $f_c \gg f_p$:

$$2\left(\frac{f_R - f_H}{f_R + f_H}\right) \simeq \frac{f_c}{f_p} \qquad f_p \gg f_c \tag{3a}$$

$$2\left(\frac{f_R - f_H}{f_R + f_H}\right) \simeq 3\left(\frac{f_p}{f_c}\right)^2 \qquad f_c \gg f_p \tag{3b}$$

It is also useful to compute the normalized maximum bandwidth of the Z mode in the same two limits:

$$2\left(\frac{f_H - f_L}{f_H + f_L}\right) \simeq \frac{f_c}{f_p} \qquad f_p \gg f_c \tag{4a}$$

$$2\left(\frac{f_H - f_L}{f_H + f_L}\right) \simeq 2 \qquad f_c \gg f_p \tag{4b}$$

Thus when $f_p \gg f_c$, the Z mode would be an extremely narrow-band emission separated by a narrow gap from the continuum cutoff. When $f_c \gg f_p$, the Z mode could be broadband, but it would still be separated by a narrow gap from the continuum cutoff.

As we have stated earlier, the Voyager PWS instrument is unable to measure directly the polarization of either the continuum or the narrow-band emission, but recently, *Leblanc et al.* [1986] have reported polarization measurements of "continuum-like" emissions by the Voyager planetary radio astronomy experiment (PRA). The PRA determines wave polarization by measuring the phase difference between signals in the two Voyager antennas, which have an angular separation of 90°. This is possible for the PRA, which employs the antennas as two monopoles, while the PWS uses the same antennas as a single dipole. *Leblanc et al.* [1986] have identified emissions occurring in the 1.2-kHz PRA channel as continuum and determined that the waves are primarily left-hand polarized. Unfortunately, the bandwidth of their 1.2-kHz channel is about 1 kHz, and the PWS wideband data presented here reveal the complexity of the wave spectrum in this frequency range. Consequently, it is difficult to ascertain to which wave mode their results apply. For example, the Z mode in regions 6 and 7 of the CMA diagram can be left-hand polarized, so it is not clear that the *Leblanc et al.* [1986] results apply to the lower-frequency border of the continuum band.

4. Spatial Distribution of Z Mode Observations

The narrow line in Figure 4 shows the trajectory of Voyager 1 plotted in Jovian magnetic dipole coordinates for the period of time that Voyager 1 was within 80 R_J of Jupiter. The distance Z above the magnetic dipole equator is plotted against L, the distance from the center of the planet at which the Voyager 1 field line crosses the magnetic equatorial plane. Both distances are expressed in units of Jovian radii (R_J). The open circles denote the time 0000 spacecraft event time (SCET) on successive days of the year 1979, with the day number indicated next to each circle. The heavier lines indicate where Z mode emissions were found in the majority of

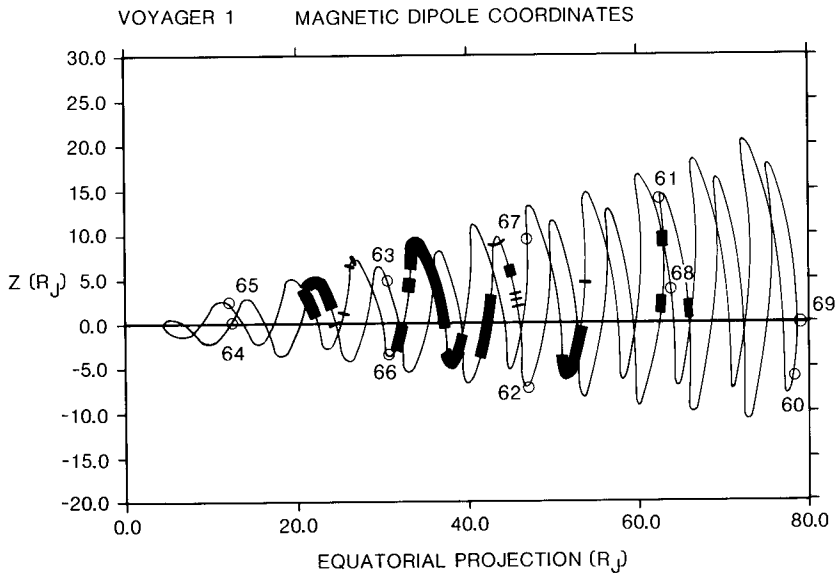

Fig. 4. Z mode spatial occurrence: Voyager 1. The narrow line shows the trajectory of Voyager 1 in Jovian magnetic dipole coordinates. The distance Z (in Jovian radii) above the magnetic dipole equator is plotted against L, the distance in Jovian radii from Jupiter's center at which the Voyager 1 field lines cross the equator. The open circles denote the time 0000 SCET on successive days of the year 1979. The day number is indicated near each open circle. The heavier lines superposed on the trajectory curves indicate where Z mode emissions were found in the majority of the wideband frames acquired during the given period of time.

wideband frames in the given time interval. Figure 5 is the corresponding plot for Voyager 2.

The data shown in Figures 4 and 5 were not normalized to the duration of each event or to the rate of acquisition of 48-s wideband frames in any time period, nor have we made a complete search of all 11,000 wideband frames for Z mode events. Thus Figures 4 and 5 cannot represent occurrence probabilities and are intended only to convey a visual impression of where we happened to find Z mode radiation. Nonetheless, we can draw one conclusion: Z mode radiation is a common feature of Jupiter's middle magnetosphere. All the events shown occurred between 20 and 60 R_J (one event, not shown, was found at 90 R_J), and there is no apparent dependence on the distance Z. The fact that no Z mode radiation was found within 20 R_J may reflect the fact that $f_p \gg f_c$ there, so that the gap between the continuum cutoff at f_R and

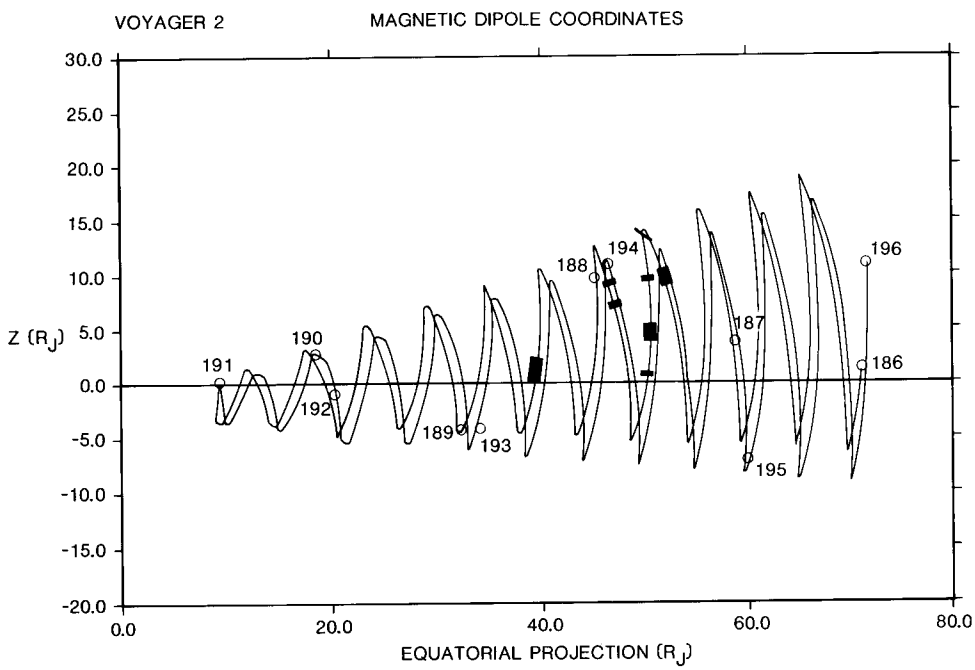

Fig. 5. Z mode spatial occurrence: Voyager 2. This plot is the Voyager 2 analog of Figure 4.

the Z mode below f_H narrows and becomes difficult to spot. Similarly, we may not have found Z mode emissions in regions where $f_c \gg f_p$, such as the lobes of Jupiter's magnetic tail.

5. Plasma Sheet Crossing of March 8, 1979: Properties of Z Mode Radiation at a Possible Source

Plate 6 shows a composite frequency-time display of plasma wave data formed by joining together the spectra from numerous 48-s wideband frames. The small white bars at the top of each panel of Plate 6 indicate the time periods for which 48-s wideband data were acquired. The spaces between the white bars were filled in by making 48-s average spectra for each frame acquired and interpolating in the intervals where no data were collected. The top panel of Plate 6 shows a fully interpolated data display, whereas those periods where the intervals between acquired data frames were sufficiently long to render the interpolation questionable were deleted in the bottom panel of Plate 6.

Voyager 1 traversed the nightside plasma sheet during the time interval shown in Plate 6. The plasma sheet crossing is immediately evident in the rapid increase in the lower continuum cutoff frequency beginning near 0600 SCET, which we attribute to an increase in the electron density. The continuum cutoff frequency rose to a peak of about 2 kHz near 0622 SCET and then diminished, and Voyager 1 exited the plasma sheet at 0645 SCET. An intense Z mode band was found on either side of the plasma sheet but not inside it.

Figure 6 presents a more detailed view of the plasma sheet crossing in Plate 6. The middle panel, which shows the time profile of the magnetic field from about 0552 SCET to 0648 SCET, confirms our identification of a plasma sheet crossing. The eight surrounding panels show portions of wideband data frames acquired at the times indicated. The frequency scales of these panels have been adjusted so as to contain the lower-frequency cutoff of the continuum radiation. Panels 3, 4, 5, and 6, which were acquired within the plasma sheet, contain little or no Z mode radiation, while panels 1 and 2 and 7 and 8, which were acquired at the edges of the plasma sheet, clearly display an intense Z mode band. Since $f_p \gg f_c$ inside the plasma sheet, (3) and (4) suggest that Z mode radiation would be concentrated in a narrow band very near the lower cutoff of the continuum. The features below the continuum on panels 3, 4, 5, and 6 do not have this character and are not in the Z mode.

The top panel of Plate 7 shows a frequency-time display for the time interval corresponding to panel 2 of Figure 6, during which the Z mode radiation terminated on the inbound pass into the plasma sheet. Figure 7 shows the magnetic field data for the first 24 s of the 48-s wideband display. The continuum cutoff increased from below 750 Hz to above 1000 Hz during these first 24 s, while the magnetic field strength decreased from 17.5 γ at $t = 0$ s to 16 γ at $t = 24$ s, presumably owing to an increase in plasma pressure. The Z mode radiation disappeared precisely when the continuum cutoff frequency was increasing the most rapidly. Note that just before it disappeared, the Z mode increased in intensity, as evidenced by the apparent disappearance of the continuum owing to the AGC effect.

The left-hand panel of Figure 8 shows 4-s average spectral densities, in V^2/m^2-Hz, obtained from electric field channel data, for the intervals 0–4 s, 8–12 s, and 16–20 s, in Plate 7. These intervals, which we label as 1, 2, and 3, respectively, correspond to times when the Z mode and the continuum appeared together in the wideband frames, when the Z mode was so intense that it triggered the AGC filter, and when only the continuum appeared. All three spectra had the same amplitude above 1.78 kHz, showing that the continuum amplitude actually remained constant and that all the variations in the frequency-time spectrogram were due to variations in the Z mode spectral density. The 562-Hz spectral density rose from 6×10^{-12} (interval 1) to 1.2×10^{-10} (interval 2) and then dropped to 1.5×10^{-14} (interval 3); thus the 562-Hz spectral density increased by a factor of 20 and then decreased by a factor of 10,000, all in the brief period of 20 s. Earlier, the 562-Hz spectral density had varied over the range 10^{-11} to 10^{-9}, in the last 4 min before the Z mode radiation disappeared.

The right panel of Figure 8 presents the same spectral information in a format designed to illuminate the relative energy densities in the Z mode and continuum bands. To this end, we multiplied the electric field spectral density by the channel frequency, f, divided by 8π, and converted to units of ergs per cubic centimeter. This method of data display is often used in astrophysics, because it enables one to estimate at a glance the relative energy densities in logarithmic frequency intervals. The energy densities in the Z mode and continuum bands were roughly equal in time interval 1, when both bands were visible in the frequency-time spectrogram; the energy density in the Z mode band was roughly a factor of 30 larger in interval 2. The largest Z mode energy density encountered on the approach to the plasma sheet was about 200 times that of the continuum.

Having established that all three spectral densities are the same above 1.78 kHz, we may now estimate the peak spectral density in the Z mode band more accurately. Figure 9 shows individual 4-s average spectra acquired by the wideband system for the intervals 1, 2, and 3. The AGC effect has been removed by requiring the spectral densities to be the same at 1.78 kHz for all three intervals. The peak of the Z mode band was about half-way between the 310-Hz and 562-Hz channels of the plasma wave spectrometer, so that neither channel obtained an accurate measurement of the peak spectral density. The peak Z mode spectral density actually exceeded 10^{-9} V^2/m^2-Hz during interval 2.

Using the magnetic field data in Figure 7 and the detailed spectra in Figure 9, we can now solve for the characteristic frequencies pertinent to the first and second time intervals, assuming that the low-frequency cutoff of the continuum is f_R. These frequencies are indicated by solid circles and are labeled by R, H, P, C, and L in decreasing order of frequency. The electron cyclotron frequency was about 475 Hz during interval 1, and we estimate the right-hand cutoff frequency to have been 620 Hz, as indicated. From these values it follows that f_L was 145 Hz, f_p was 300 Hz, and f_H was 560 Hz. Approximately 4 s later, in interval 2, f_R had increased to about 750 Hz, and f_c had decreased to 465 Hz. It follows that f_p increased to 464 Hz (so that the electron density had increased by about a factor of 2.4), f_H increased to 625 Hz, and f_L increased to 250 Hz. Thus in interval 1 the ratio f_p/f_c was about 0.6; when the Z mode band was its most intense, f_p/f_c was about unity, and as f_p/f_c increased further, the Z mode disappeared. The Z mode spectral density peaked at the electron cyclotron frequency in both intervals.

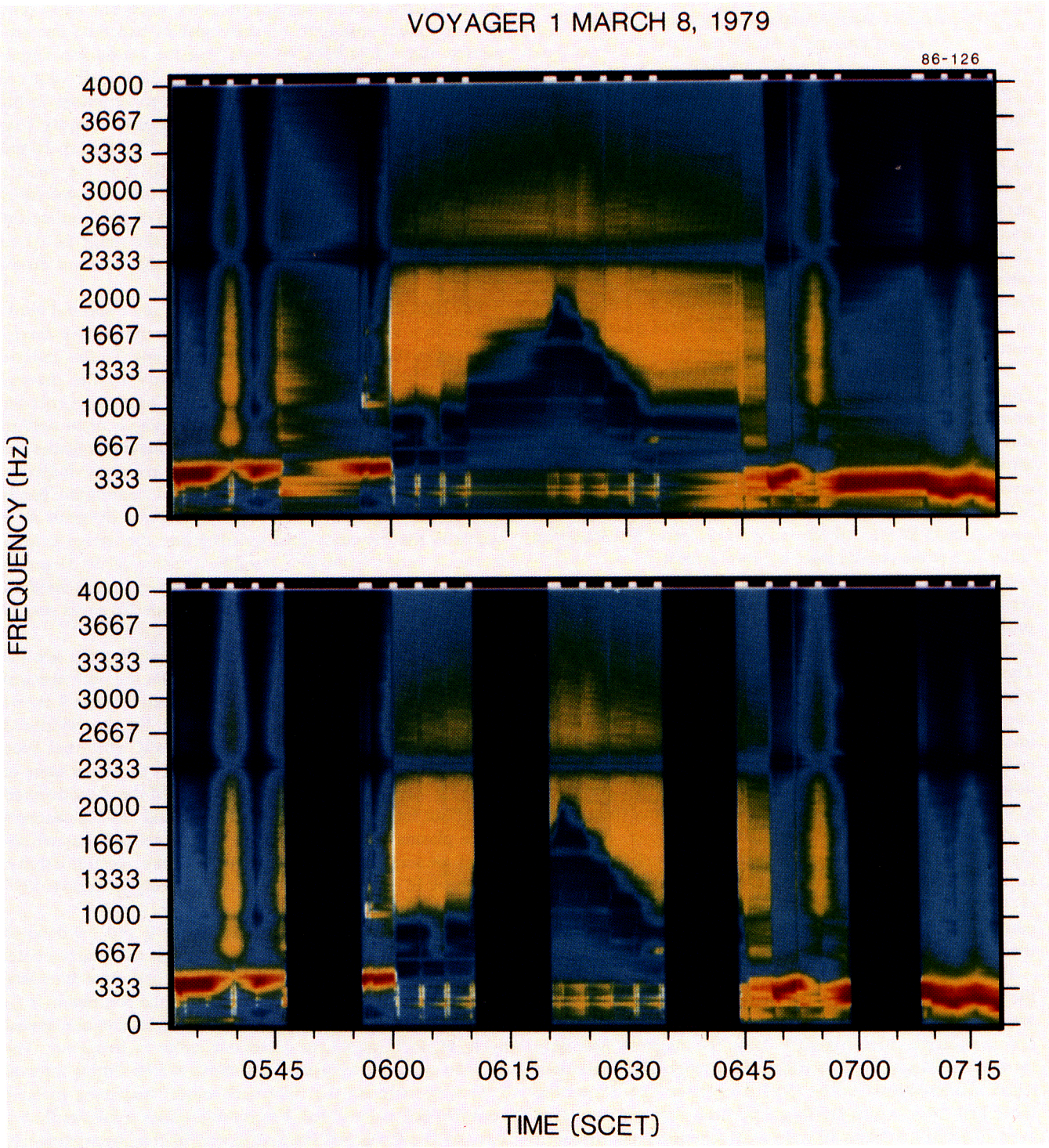

Plate 6. Plasma sheet crossing on March 8, 1979: an overview. The small white bars at the tops of both panels indicate periods where a continuous sequence of 48-s wideband data frames was acquired. The spectra were mathematically interpolated in the intervening periods in which no data were acquired to synthesize a frequency-time display that extends from 0537-0719 SCET. Voyager 1 passed through the plasma sheet during this interval. The top panel shows a fully interpolated frequency-time display, whereas the regions where we believe the interpolation is unreliable have been deleted in the bottom panel.

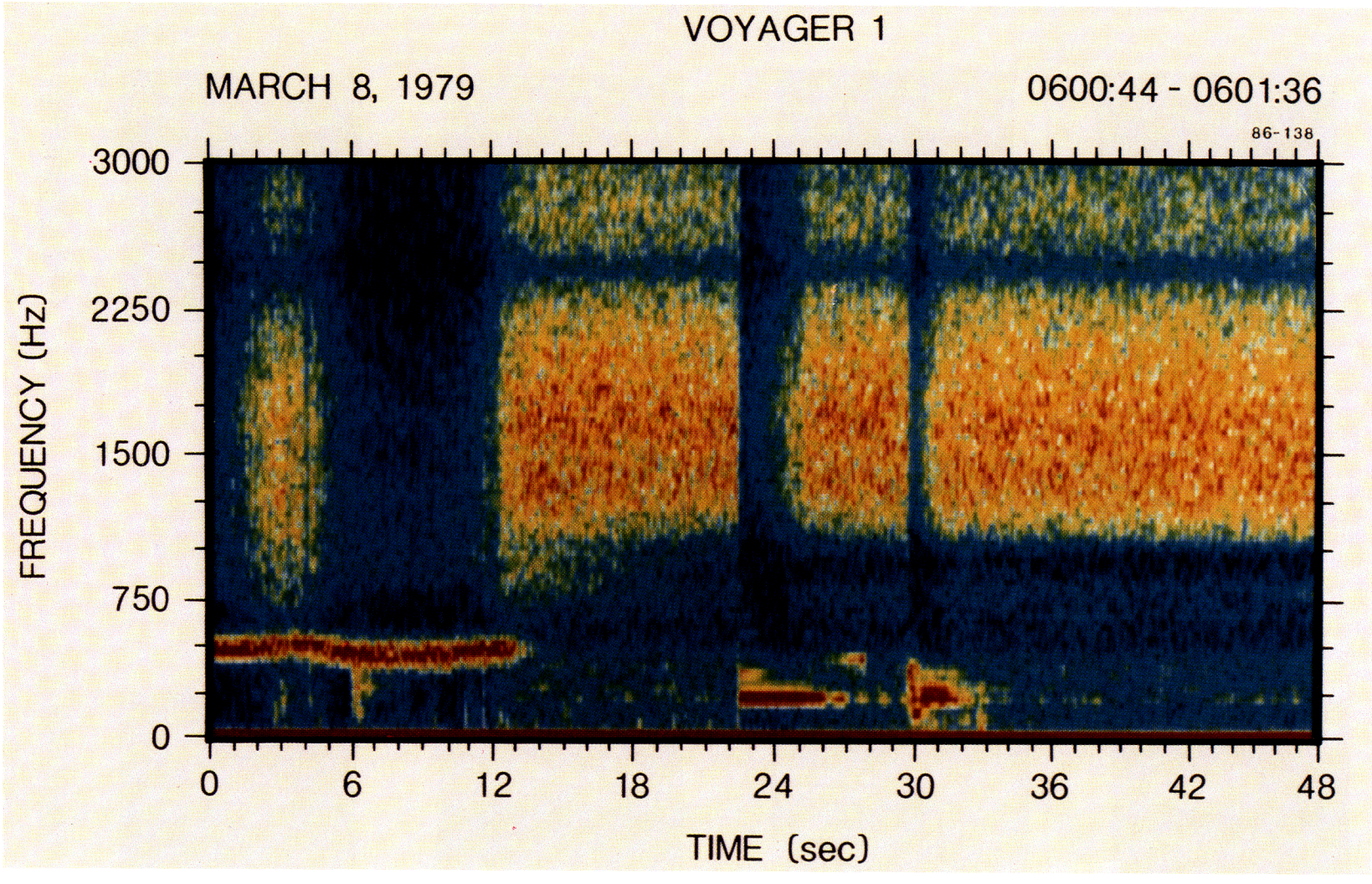

Plate 7. Abrupt Z mode termination at a density gradient. Panel 2 of Figure 6 is the last measurement of Z mode radiation that Voyager 1 made as it entered the plasma sheet. The radiation suddenly stopped just as the lower cutoff of the continuum increased, presumably at a strong density gradient. This plate shows a color spectrogram of the same event. Just before the Z mode emission terminated, it intensified and became so strong that the AGC blanked out the continuum.

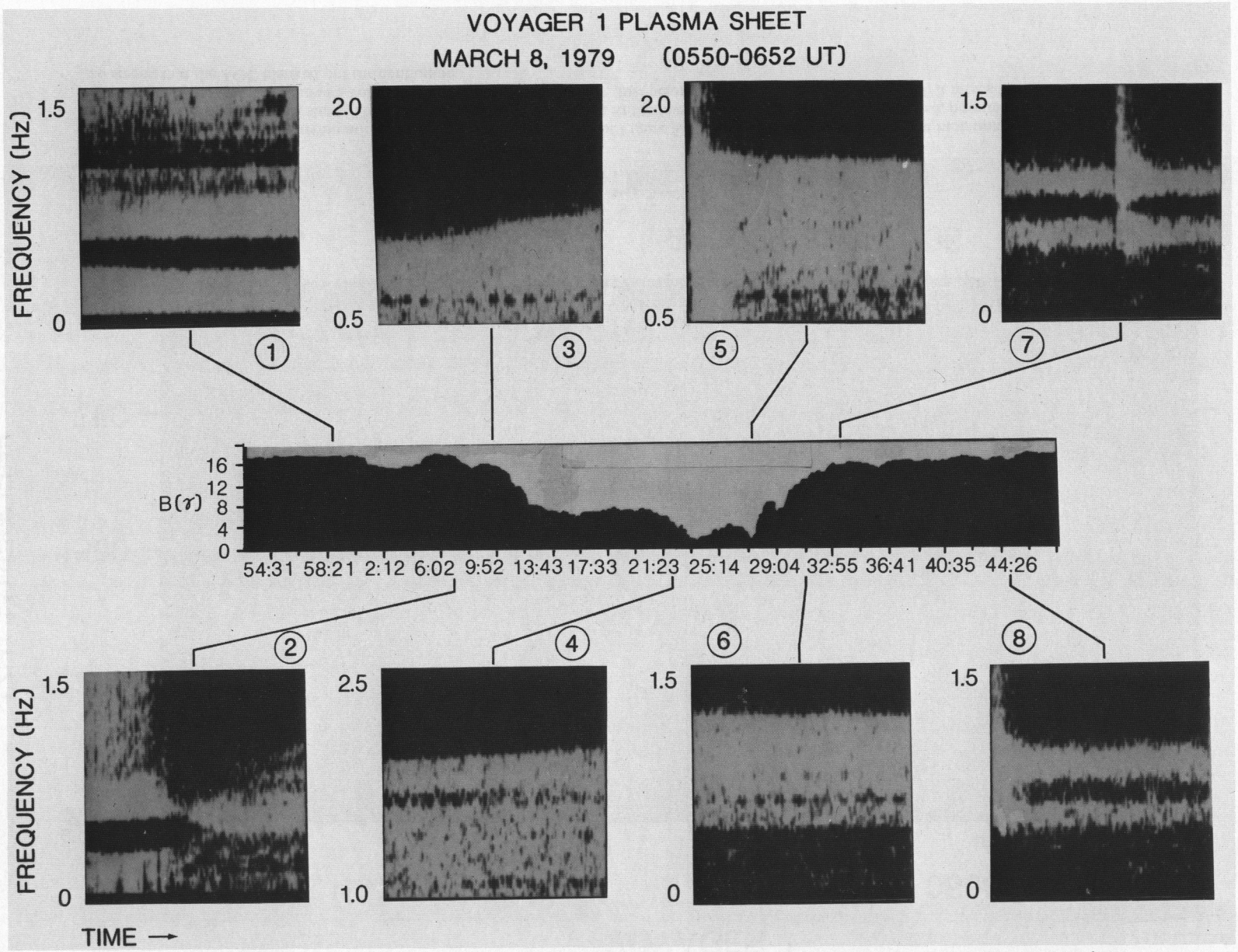

Fig. 6. Plasma sheet crossing on March 8, 1979: a closer view. The central panel shows the magnetic field data measured between about 0552 and 0648 SCET, confirming that Voyager 1 crossed the plasma sheet. The magnetic field is measured in units of 1 $\gamma = 1$ nT $= 10^{-5}$ G. The eight surrounding panels show snapshots of the wideband plasma wave data taken at the times indicated. The frequency range of each snapshot (0–1.5 kHz to 1.0–2.5 kHz) has been adjusted to include the lower cutoff of the continuum. Strong Z mode radiation appears at the outer edges of the plasma sheet (panels 1 and 2 and 7 and 8). The Z mode is not apparent inside the plasma sheet (panels 3, 4, 5, and 6). The line at 1.5 kHz in panel 4 is probably an artifact.

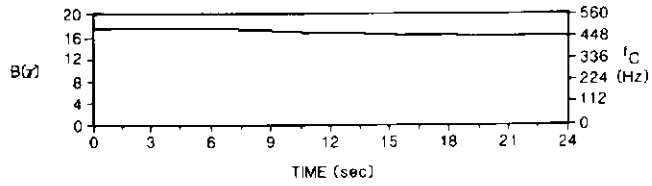

Fig. 7. This figure shows the magnetic field strength measured during the interval $t = 0$–24 s of the wideband frame in Plate 7. The magnetic field strength decreased from 17.5 γ at $t - 0$ to 16 γ at $t - 24$ s.

6. Summary and Discussion

This paper presents initial results of a survey of PWS wideband frames that exhibit a narrow-band emission below the low-frequency cutoff of the continuum band. These waves were first reported by *Gurnett et al.* [1980], and our analysis of over 400 wideband frames has enabled us to identify them as the Z mode.

It is unlikely that the narrow-band emissions are electrostatic waves, since their frequencies have no apparent relationship to the electron cyclotron frequency, its harmonics, or variations in the magnetic field strength. If they are electromagnetic waves, then their identity might be revealed by comparing their frequencies and bandwidths with solutions of the cold-plasma, electromagnetic dispersion relation. In the absence of precise plasma densities from the PLS for each frame, we have tested two different interpretations of the continuum cutoff frequency to determine f_p. The data are organized best when the continuum cutoff is chosen to be f_R; then the narrow-band emission consistently lies below f_H and above f_L. The significance of this result is twofold. First, the narrow-band emission is probably the Z mode. Second, in order for a gap to exist between f_R and f_H, the continuum must be devoid of L-O mode waves at low frequencies.

This interpretation of the continuum cutoff has major consequences for the implied composition of continuum radiation at Jupiter. If the continuum were pure L-O mode, it would not be present below the plasma frequency. A Z mode superposed on the L-O continuum would extend above and below the lower-frequency border of the L-O continuum. If the continuum were an equal mixture of R-X and L-O mode, its intensity would diminish by half at the right-hand cutoff frequency and disappear at the plasma frequency. A Z mode emission superposed on an R-X, L-O continuum would again overlap the lower-frequency border of the continuum band. If the lower border of the continuum were pure R-X mode, the continuum would disappear at the right-hand cutoff frequency. In this case a Z mode emission would appear as a narrow band between the left-hand cutoff and upper hybrid frequencies, separated by a distinct gap from the R-X continuum band. Thus the Z mode and the continuum will be separated by a gap only if the continuum is R-X mode. This is quite unlike terrestrial continuum radiation, which is a nearly equal mixture of R-X and L-O mode waves. Our results also directly address the concerns of *Gurnett et al.* [1981], who based their estimates of the density in Jupiter's magnetosphere on the assumption that the continuum cuts off at the local plasma frequency, namely, that the continuum contains L-O mode and that there is no lower-frequency cutoff on the propagation path between the radiation source and the spacecraft.

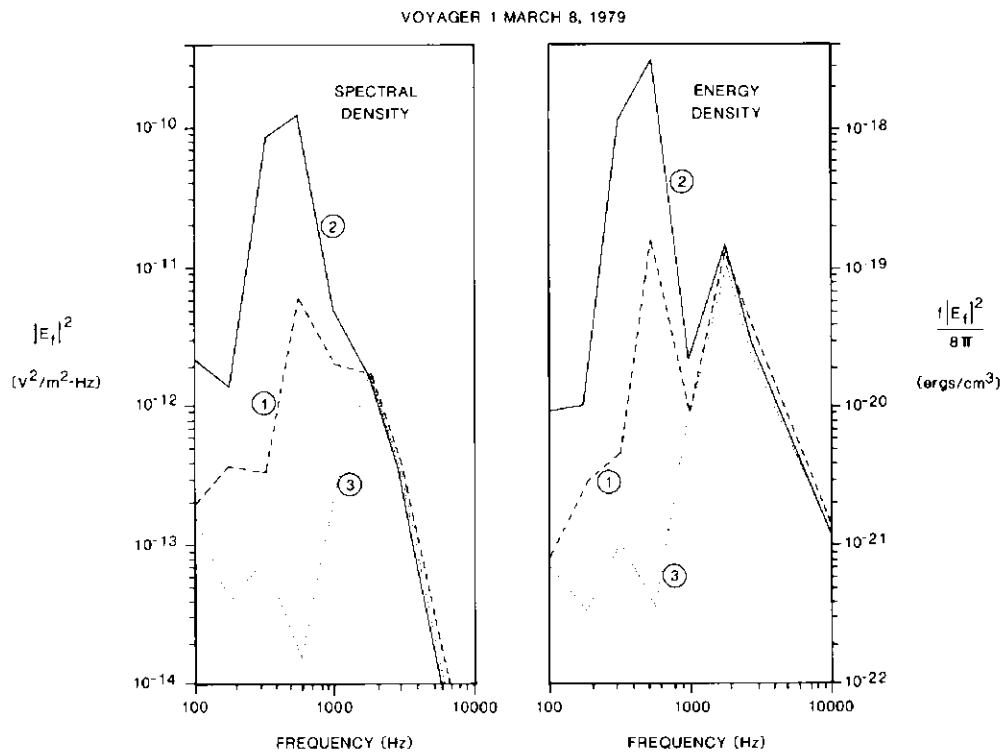

Fig. 8. Wave spectral and energy densities obtained from channel data. The left-hand panel shows the 4-s average spectral density measured by the 16-channel spectrometer for the times $t = 0$ 4, 8 12, and 16–20 s, labeled as 1, 2, and 3, respectively. The right panel shows the same data, now plotted as an energy density, which was obtained by multiplying the spectral density by the frequency, dividing by 8 π, and converting to units of ergs per cubic centimeter.

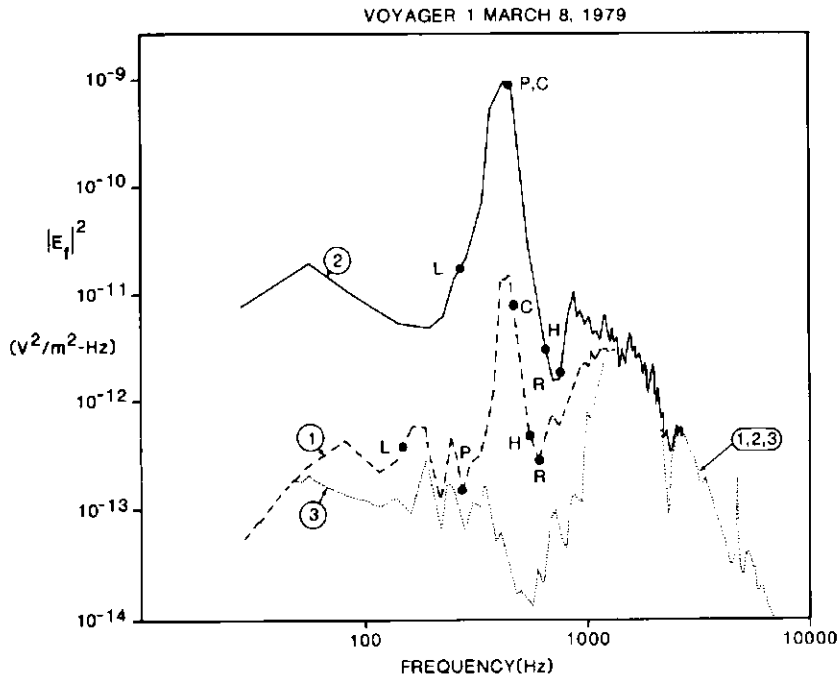

Fig. 9. Wave spectral densities and characteristic frequencies obtained from wideband data. This figure shows the spectral densities obtained from wideband data for the same three time intervals as in Figure 8. The AGC effect was removed by requiring all three spectra to have the same density at 1.78 kHz. The peak of the Z mode was between the 311- and 562-Hz channels, so that neither one measured the peak spectral density accurately. The CMA solutions for the intervals $t = 0$ 4 and 8 12 s are indicated by solid circles and labeled as in Plate 2.

For the events we studied here, their caveat about the composition of the continuum was justified, which suggests that the plasma density estimates obtained earlier may need modifications when the electron cyclotron and plasma frequencies are comparable, such as, for example, in the lobes of Jupiter's magnetic tail.

The only conclusive way to determine the wave modes composing the continuum spectrum is to measure the wave polarization. The dipole antenna of the PWS instrument can only determine the wave polarization when the spacecraft rotates; however, since the Voyager spacecraft are three-axis stabilized, this only occurs during scheduled maneuvers. The planetary radio astronomy (PRA) receiver does measure wave polarizations at 1.2 kHz through two monopole antennas, but it does not have the frequency resolution to differentiate between the continuum and the Z mode bands.

We cannot draw the conclusion that the Jovian continuum never contains L-O mode radiation. First of all, it is possible that L-O mode is present in the Jovian continuum, but not at the low-frequency cutoff. Moreover, our data were selected because a gap separated the continuum band from the Z mode band, and the CMA diagram tells us that L-O mode radiation must be absent for this to happen. Thus we can only say that L-O mode radiation is sometimes absent from the low-frequency Jovian continuum but may very well be present at other times. Indeed, *Moses et al.* [1987] have studied an event in which a roll maneuver enabled a measurement of the polarization of the waves near the lower-frequency cutoff of the continuum band. They found that region 6a L-O mode radiation was present in the continuum down to the plasma frequency and that a region 7 Z mode extended to lower frequencies. Their measurements of the Z mode were in the lobes of Jupiter's magnetic tail, where $f_c \gg f_p$, corresponding to a different region of the CMA diagram than did the Z mode radiation in the present study.

We also cannot say that we have found all the types of Z mode events in Jupiter's magnetosphere. Not only can we have missed those that occur in conjunction with an L-O continuum component, but we selected events for which electron plasma and cyclotron frequencies were comparable. We may have missed events within 20 R_J, or deep in Jupiter's magnetic tail, where f_p/f_c is not near unity.

We may estimate the strength parameter of the Z mode electric field for the March 8, 1979, plasma sheet crossing to be

$$\frac{E^2}{8\pi n T_e} \simeq \frac{2 \times 10^{-4}}{T_e(\text{eV})} \tag{5}$$

where we took the electric field energy density to be about one-half the peak value at 562 Hz in interval 2 and inserted our measured electron density, $n \approx 4 \times 10^{-3}$ cm^{-3}. The electron temperature, T_e, is expressed in units of electron volts. Since the cold electron temperature is typically 50–160 eV at the outer edges of the Jovian plasma sheet [*Scudder et al.*, 1981; E. C. Sittler, private communication, 1986], the Z mode strength parameter was at least 10^{-6} just before Voyager 1 entered the plasma sheet. It rose above 10^{-4} on the approach to the plasma sheet.

These Z mode strength parameters are comparable with those typically found for electrostatic waves, which are usually 10^{-5} or smaller. This is particularly impressive given that the electromagnetic Z mode has phase and group speeds near the speed of light, whereas electrostatic waves propagate slowly. The Z mode strength parameter can be much larger still in the low-density lobes well away from the plasma sheet, where the electron density is at least an order of magnitude smaller, and

the Z mode energy density at very low frequencies is even larger [*Moses et al.*, 1987].

The observations reported in section 5 may have some bearing on how and where the Z mode is generated. The extreme intensification of wave energy in the Z mode band near the edge of the plasma sheet coupled with absence of Z mode radiation in the sheet strongly suggests that the boundary between tail lobe and plasma sheet is a Z mode generation region. The plasma sheet is known to be a region with enhanced densities of higher-energy particles [*Scudder et al.*, 1981; *Krimigis et al.*, 1981] which possibly provide the free energy for wave generation. The Z mode radiation spectrum near this possible generation region peaked at the electron cyclotron frequency and was the most intense when the electron cyclotron frequency equaled the plasma frequency. It is unlikely that it propagated directly from a source that originally generated electrostatic upper hybrid waves, as *Lembege and Jones* [1982] have proposed for the production of continuum, since no electrostatic activity at the upper hybrid frequency was detected. *Budden and Jones* [1987] have recently extended the theory of the generation of terrestrial continuum radiation by the linear conversion of Z mode radiation in density gradients.

It has been suggested that terrestrial Z mode radiation [*Gurnett et al.*, 1983] might be generated by the cyclotron maser instability [*Wu and Lee*, 1979; *Wu*, 1981; *Wu et al.*, 1981, 1982; *Dusenberry and Lyons*, 1982; *Hewitt et al.*, 1982, 1983; *Melrose et al.*, 1982; *LeQueau et al.*, 1984; *Omidi and Gurnett*, 1982; *Omidi et al.*, 1984; *Pritchett*, 1984*a*, *b*]. Most of the instability calculations have been motivated by observations of terrestrial kilometric radiation, which is thought to be generated in regions where $f_p \ll f_c$. The calculations of *Hewitt et al.* [1983] and *Melrose et al.* [1982] are particularly pertinent to our observations. Using mildly relativistic electron distribution functions appropriate to terrestrial auroral field lines, *Melrose et al.* [1982] calculated and compared the convective and nonconvective growth roles of obliquely propagating X, O, and Z modes. They found that the X mode dominated when $f_p < \frac{1}{3} f_c$; when $f_p > \frac{1}{3} f_c$, the Z mode had the largest convective growth rate. However, *Hewitt et al.* [1983] found that the Z mode was generated between f_c and f_H, whereas the Z mode at the plasma sheet outer boundary in Plate 7 and Figures 7, 8, and 9 was more or less symmetrically peaked at the electron cyclotron frequency. Thus while *Melrose et al.* [1982] predict that Z mode will be preferentially generated when $f_p \approx f_c$, which is consistent with our observations, their predicted frequency band differs from what we observed in at least one case. We also note that some of the events in Figure 3 had $f \gg f_c$; however, these may have been detected away from their source regions. In order to pursue this topic further, it will be necessary to ascertain whether the mildly relativistic electrons near the boundaries of the Jovian plasma sheet have free-energy sources appropriate for wave growth and to perform more realistic instability calculations that are suited to the Jovian environment.

Our study raises many more questions. For example, the continuum is always present in Jupiter's magnetosphere, and its spectral distribution above its lower-frequency cutoff is gently modulated with 5- and 10-hour periods [*Kurth et al.*, 1986]. In contrast, the Z mode is sometimes present for tens of minutes and sometimes comes and goes on time scales of seconds. The power flux of the Z mode varies by at least 4 orders of magnitude, and its integrated power can sometimes exceed that of the continuum by an order of magnitude or more; sometimes, it is energetically insignificant in relation to the continuum. Are the intermittency of Z mode events and their variable intensity due to variability at the Z mode source(s) or to variable propagation conditions between the source(s) and the spacecraft? The plasma sheet is probably not the only source of Z mode radiation, because the Z mode radiation in the lobes of the magnetic tail has a frequency much below that encountered at the edges of the plasma sheet. What are the source(s) of tail lobe Z mode and continuum radiation? When is the L-O mode a part of the Jovian continuum, and when is it not? These questions remain for the future.

Acknowledgments. We are indebted to R. P. Lepping for providing data from the magnetometers onboard Voyagers 1 and 2 and to D. Barbosa and R. Walker for their help in displaying these data. We thank D. Jones for illuminating discussions. This research was supported at TRW by contract NAS5-28703 and at the University of Iowa by contract 954013.

The Editor thanks M. D. Desch and D. Jones for their assistance in evaluating this paper.

REFERENCES

Budden, K. G., and D. Jones, Conversion of electrostatic upper hybrid emissions to electromagnetic O and X mode waves in the earth's magnetosphere, *Ann. Geophys. Gauthier Villars*, *5*, 21, 1987.

Dusenberry, P. B., and L. R. Lyons, General concepts on the generation of auroral kilometric radiation, *J. Geophys. Res.*, *87*, 7476, 1982.

Gurnett, D. A., and R. R. Shaw, Electromagnetic radiation trapped in the magnetosphere above the plasma frequency, *J. Geophys. Res.*, *78*, 8136, 1973.

Gurnett, D. A., W. S. Kurth, and F. L. Scarf, The structure of the Jovian magnetotail from plasma wave observations, *Geophys. Res. Lett.*, *7*, 553, 1980.

Gurnett, D. A., F. L. Scarf, W. S. Kurth, R. R. Shaw, and R. L. Poynter, Determination of Jupiter's electron density profile from plasma wave observations, *J. Geophys. Res.*, *86*, 8199, 1981.

Gurnett, D. A., S. D. Shawhan, and R. R. Shaw, Auroral hiss, Z mode radiation, and auroral kilometric radiation in the polar magnetosphere: DE 1 observations, *J. Geophys. Res.*, *88*, 329, 1983.

Hewitt, R. G., D. B. Melrose, and K. G. Ronnmark, The loss-cone driven electron-cyclotron maser, *Aust. J. Phys.*, *35*, 447, 1982.

Hewitt, R. G., D. B. Melrose, and G. A. Dulk, Cyclotron maser emisson of auroral Z mode radiation, *J. Geophys. Res.*, *88*, 10,065, 1983.

Krimigis, S. M., J. F. Carbary, E. P. Keaty, C. G. Bostrom, W. I. Axford, G. Gloeckler, L. J. Lanzerotti, and T. P. Armstrong, Characteristics of hot plasma in the Jovian magnetosphere: Results from the Voyager spacecraft, *J. Geophys. Res.*, *86*, 8227, 1981.

Kurth, W. S., D. A. Gurnett, and F. L. Scarf, Periodic amplitude variations in Jovian continuum radiation, *J. Geophys. Res.*, *91*, 13,523, 1986.

Leblanc, Y., D. Jones, and H. O. Rucker, Jovian 1.2-kHz nonthermal continuum radiation, *J. Geophys. Res.*, *91*, 9995, 1986.

Lembege, B., and D. Jones, Propagation of electrostatic upper hybrid emission and Z mode waves at the geomagnetic equatorial plasma pause, *J. Geophys. Res.*, *87*, 6187, 1982.

LeQueau, D., R. Pellat, and A. Roux, Direct generation of the auroral kilometric radiation by the maser synchrotron instability: An analytical approach, *Phys. Fluids*, *27*, 247, 1984.

Melrose, D. B., K. G. Ronnmark, and R. G. Hewitt, Terrestrial kilometric radiation: The cyclotron theory, *J. Geophys. Res.*, *87*, 5140, 1982.

Moses, S. L., W. S. Kurth, C. F. Kennel, F. V. Coroniti, and F. L. Scarf, Polarization of low-frequency electromagnetic radiation in the lobes of Jupiter's magnetotail, *J. Geophys. Res.*, *92*, 4701, 1987.

Omidi, N., and D. A. Gurnett, Growth rate calculations of auroral kilometric radiation using the relationship resonance condition, *J. Geophys. Res.*, *87*, 2377, 1982.

Omidi, N., C. S. Wu, and D. A. Gurnett, Generation of auroral kilometric and Z mode radiation by the cyclotron maser mechanism, *J. Geophys. Res.*, *89*, 883, 1984.

Prichett, P. L., Relativistic dispersion and the generation of auroral kilometric radiation, *Geophys. Res. Lett.*, *11*, 143, 1984*a*.

Pritchett, P. L., Relativistic dispersion, the cyclotron maser instability and auroral kilometric radiation, *J. Geophys. Res.*, *89*, 8957, 1984*b*.

Scarf, F. L., D. A. Gurnett, and W. S. Kurth, Measurements of plasma wave spectra in Jupiter's magnetosphere, *J. Geophys. Res.*, *86*, 8181, 1981.

Scudder, J. D., E. C. Sittler, Jr., and H. S. Bridge, A survey of the plasma electron environment of Jupiter: A view from Voyager, *J. Geophys. Res.*, *86*, 8157, 1981.

Shaw, R. R., and D. A. Gurnett, A test of two theories for the low-frequency cutoff of nonthermal continuum radiation, *J. Geophys. Res.*, *85*, 4571, 1980.

Stix, T. H., *The Theory of Plasma Waves*, McGraw-Hill, New York, 1962.

Wu, C. S., The source mechanism of auroral kilometric radiation, in *Physics of Auroral Arc Formation*, *Geophys. Monogr. Ser.*, vol. 25, edited by S.-I. Akasofu and J. R. Kan, pp. 418–427, AGU, Washington, D. C., 1981.

Wu, C. S., and L. C. Lee, A theory of terrestrial kilometric radiation, *Astrophys. J.*, *230*, 621, 1979.

Wu, C. S., C. S. Lin, H. K. Wang, S. T. Tsai, and R. L. Zhou, Absorption and emission of extraordinary mode electromagnetic waves near cyclotron frequency in nonequilibrium plasmas, *Phys. Fluids*, *24*, 2191, 1981.

Wu, C. S., H. K. Wong, D. J. Gorney, and L. C. Lee, Generation of auroral kilometric radiation, *J. Geophys. Res.*, *87*, 4476, 1982.

F. F. Chen, R. F. Chen, F. V. Coroniti, C. F. Kennel, S. L. Moses, and F. L. Scarf, TRW Space and Technology Group, R1/1176, One Space Park, Redondo Beach, CA 90278.

W. S. Kurth, Department of Physics and Astronomy, University of Iowa, Iowa City, IA 52242.

(Received February 2, 1987;
revised April 10, 1987;
accepted April 30, 1987.)